Wet Mantle Transition Zone beneath the Indian shield? Constraints from P-to-S Receiver Functions Analysis

Akash Kharita[1,1] and Sagarika Mukhopadhyay[1,1]

[1]Indian Institute of Technology Roorkee

November 30, 2022

Abstract

Indian plate passed over four plumes during its way towards Eurasian plate. These interactions with plumes certainly affected the upper mantle and crust of Indian plate as manifested by its thinned lithosphere and relatively low shear velocities both in crust and upper mantle, but the depth extent of these effects of plume-lithosphere interaction remains ambiguous. In this study, we investigate the mantle transition zone beneath Indian shield using P-to-S receiver functions computed at 24 stations covering the entirety of the Indian shield to investigate the depth extent of the imprints of the plume-lithosphere interaction as well as to study the lateral variations of transition zone beneath a stable intraplate setting like the Indian shield. Our results show good agreement with the results of previous studies as well as with the tomographic models in terms of the average apparent depths of the 410 and 660 discontinuities and the transition zone thickness. However, unlike previous studies, we find a compelling evidence of a persistent mid transition zone discontinuity beneath all the stations and a low velocity layer beneath some regions. We also investigated the frequency dependence of amplitudes of receiver functions and found most of the stations showed strong dependence of amplitudes on frequency. Based on the evidence from our investigation, we demarcate the regions potentially containing relatively more weight percentage of water inside the otherwise considered 'dry' mantle transition zone. These regions should be further investigated in detail by a dense seismic network and a realistic 3-D velocity model.

Hosted file

`figures.docx` available at https://authorea.com/users/523611/articles/607622-wet-mantle-transition-zone-beneath-the-indian-shield-constraints-from-p-to-s-receiver-functions-analysis

Physics of the Earth and Planetary Interiors

Wet Mantle Transition Zone beneath the Indian shield: Constraints from P-to-S Receiver Functions Analysis

--Manuscript Draft--

Manuscript Number:	
Article Type:	Research Paper
Keywords:	Mantle Transition Zone; Receiver Functions; Plate Tectonics; Seismology; India; Mantle
Corresponding Author:	Akash Kharita INDIA
First Author:	Akash Kharita
Order of Authors:	Akash Kharita
	Sagarika Mukhopadhyay, Ph.D.
Abstract:	Indian plate passed over four plumes during its way towards Eurasian plate. These interactions with plumes certainly affected the upper mantle and crust of Indian plate as manifested by its thinned lithosphere and relatively low shear velocities both in crust and upper mantle, but the depth extent of these effects of plume-lithosphere interaction remains ambiguous. In this study, we investigate the mantle transition zone beneath Indian shield using P-to-S receiver functions computed at 24 stations covering the entirety of the Indian shield to investigate the depth extent of the imprints of the plume-lithosphere interaction as well as to study the lateral variations of transition zone beneath a stable intraplate setting like the Indian shield. Our results show good agreement with the results of previous studies as well as with the tomographic models in terms of the average apparent depths of the 410 and 660 discontinuities and the transition zone thickness. However, unlike previous studies, we find a compelling evidence of a persistent mid transition zone discontinuity beneath all the stations and a low velocity layer beneath some regions. We also investigated the frequency dependence of amplitudes of receiver functions and found most of the stations showed strong dependence of amplitudes on frequency. Based on the evidence from our investigation, we demarcate the regions potentially containing relatively more weight percentage of water inside the otherwise considered 'dry' mantle transition zone. These regions should be further investigated in detail by a dense seismic network and a realistic 3-D velocity model.
Suggested Reviewers:	Chandrani Singh chandrani.iitkgp@gmail.com
	Sandeep Gupta sandeep.ngri@gmail.com
	Naresh Kumar nkumard12@gmail.com
	J.R. Kayal Professor jrkayal@gmail.com
	Steve Roecker roecks@rpi.edu

Cover Letter

Akash Kharita

Department of Earth Sciences

Indian Institute of Technology Roorkee

01/04/2022

Dear Editor,

We would like to submit a research article titled "Wet Mantle Transition Zone beneath the Indian shield: Constraints from P-to-S Receiver Functions Analysis" for consideration for publication in the Physics of the Earth and Planetary Interiors. We declare that this work is original and is not published elsewhere, nor is it under consideration elsewhere.

In this paper, we investigate the lateral variations in the mantle transition zone and report for the first time the possibility of a wet mantle transition zone beneath certain regions of the Indian shield based on the evidence from the nature of transition zone discontinuities and their frequency dependence. We believe our findings will be of great interest to the readers of your journal.

We declare no conflicts of interest. As a corresponding author, I confirm that the manuscript has been read and approved for submission by all the named authors.

Sincerely,

Akash Kharita

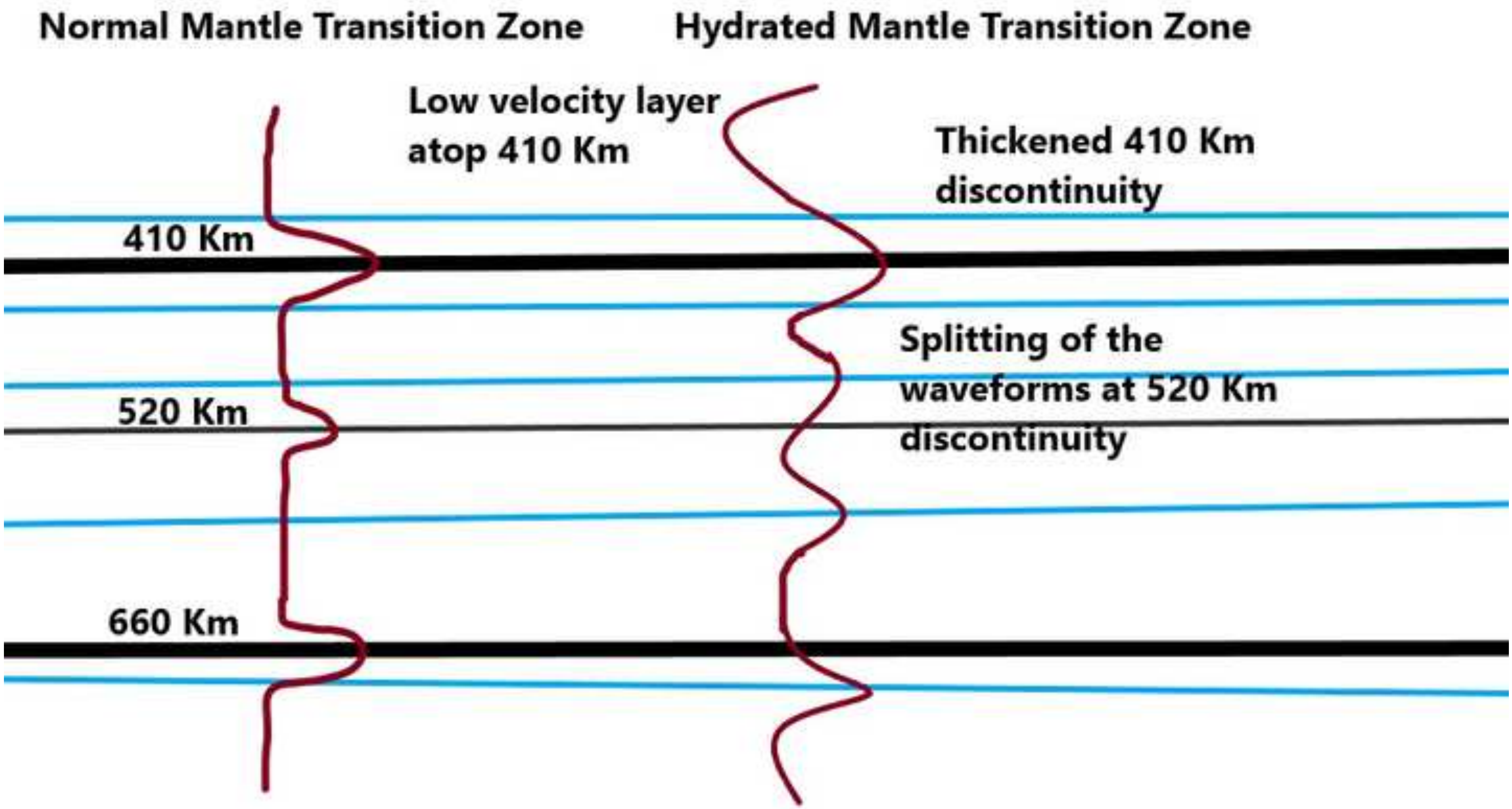
Normal Mantle Transition Zone
Hydrated Mantle Transition Zone
Low velocity layer atop 410 Km
Thickened 410 Km discontinuity
410 Km
520 Km
660 Km
Splitting of the waveforms at 520 Km discontinuity

Wet Mantle Transition Zone beneath the Indian shield: Constraints from P-to-S Receiver Functions Analysis

Akash Kharita*, Sagarika Mukhopadhyay
Department of Earth Sciences, Indian Institute of Technology Roorkee
*corresponding author – akharita1999@gmail.com

Abstract

Indian plate passed over four plumes on its way towards the Eurasian plate. These interactions with plumes certainly affected the upper mantle and crust of the Indian plate as manifested by its thinned lithosphere and relatively low shear velocities both in the crust and upper mantle, but the depth extent of these effects of plume-lithosphere interaction remains ambiguous. In this study, we investigate the mantle transition zone beneath the Indian shield using P-to-S receiver functions computed at 24 stations covering the entirety of the Indian shield to investigate the depth extent of the imprints of the plume-lithosphere interaction as well as to study the lateral variations of transition zone beneath a stable intraplate setting like the Indian shield. Our results show good agreement with the results of previous studies as well as with the tomographic models in terms of the average apparent depths of the 410 and 660 discontinuities and the transition zone thickness. However, unlike previous studies, we find ~~a~~ compelling evidence of a persistent mid-transition zone discontinuity beneath all the stations and a low-velocity layer beneath some regions. We also investigated the frequency dependence of amplitudes of receiver functions and found that most of the stations showed a strong dependence of amplitudes on frequency. Based on the evidence from our investigation, we demarcate the regions potentially containing relatively more weight percentage of water inside the other considered as a ‘dry’ mantle transition zone. These regions should be further investigated in detail by a dense seismic network and a realistic 3-D velocity model.

1 Introduction

The study of mantle structure, composition, and temperature is important for understanding the dynamics and evolution of our planet. Upper mantle is separated from the lower mantle through a transition zone lying between the approximate depths of 410 and 660 km where discontinuities in seismic velocities are observed. These discontinuities are most likely due to the solid-solid phase transition of a low-pressure Olivine (α-phase) to wadsleyite (β-phase) at 410 Km and the dislocation of Ringwoodite (γ-phase) to Magnesiowuestite and perovskite near 660 km, within the Olivine component of the mantle (Ita & Stixrude, 1992; Ringwood, 1968) . Additionally, there have been sporadic observations of another discontinuity at 520 km, believed to be caused by the β-phase to the γ-phase transition of Olivine (Deuss & Woodhouse, 2001) . Throughout the remaining text, we will refer to discontinuities at 410, 520, and 660 km as d410, d660, and d520 respectively

The Pressure-Temperature relations that govern the existence of a mineral in a given state are quantified by Clapeyron slopes. Recent studies showed a positive Clapeyron slope of +4.0 Mpa/K for the phase transition of α Olivine to β Olivine and a negative Clapeyron slope of -1 to -3 Mpa/K for the dislocation of Ringwoodite to Magnesiowuestite and Perovskite (Bina et al., 1994) . Opposite signs of the Clapeyron slope suggest that the depths of 410 and 660 discontinuities should be anticorrelated; 410 rises and 660 depress in a relatively colder transition zone whereas the opposite happens in the presence of a relatively warmer transition zone. Therefore, a thicker and a thinner MTZ can respectively indicate the presence of cold and warm thermal regions (Lebedev et al., 2002) . Additionally, the presence of water may also play a significant role in the depth of the mineralogical changes, similar to the variations caused by temperature anomalies. Previous studies have indicated that an increase of one percent increase of water in the mantle composition may lead to an increase of 14 km in the thickness of MTZ (Ghosh et al., 2013) . Study of the topography of 410, 660 and thickness of MTZ can therefore help us in constraining the thermal and chemical structure of mantle (Lebedev et al., 2002) .

The present-day Indian shield is an assemblage of Precambrian cratons (Figure 1) and records a history of long and complex tectonic evolution (Drury et al., 1984) . These cratons comprise the Aravalli (AC), Eastern Dharwar (EDC), Western Dharwar (WDC), Bastar (BC), Singhbhum (SC), and the Bundelkhand craton (BhC). The oldest rocks at the core of these cratons have been found to be in the range of 2700-3800 Ma (Meert et al., 2010) . The cratons are separated by different rift valleys believed to have formed in the Precambrian, activated in the Permian, and continued to subside in the cretaceous (Kumar, 1985) .

The breaking up of the Gondwana supercontinent at about 130 Mya (Gaina et al., 2007) created two continents – Africa in the west and a mosaic of Madagascar, Australia, Antarctica, and India in the east. Australia and Antarctica rifted apart during 128-130 Myr and Madagascar separated from India at about 90 Mya. Plate reconstructions based on the paleomagnetic data suggest that the Indian plate then continued moving NNE-ward during 85-55 Myr at a relatively very high rate of about 18-20 cm/yr (McKenzie & Sclater, 1971) . This relatively fast speed of drifting is attributed to the increased efficiency of the ridge push and slab pull effect on a thinned lithosphere possibly caused by the passage of the Indian plate over multiple plumes (Reunion, Marion, Crozet, and Kerguelen) (Kumar et al., 2007) . During its passage over the Reunion hotspot at about 65 Mya (Morgan, 1981) , Deccan volcanism began with the opening of an eruptive centre near modern-day Bombay and large-scale flooding of basaltic lava continued for about 1 Mya. The Deccan traps are currently spread across an area of about 500,000 km^2 and are one of the largest provinces of flood basalts in the world (Jay & Widdowson, 2008) . The fast-moving Indian plate collided with the Eurasian plate at about 55 Mya. The northward drifting of the Indian plate continued but with much lower speeds of about 4 cm/yr (Molnar, 1990) and the northern Indian lithosphere continued subducting beneath the Tibetan plate. The subducted part is buried beneath modern-day Tibet and is now overridden by the Eurasian plate (Replumaz et al., 2004; Van Der Voo et al., 1999) .

Indian crust and upper mantle structure have been repeatedly studied using a variety of seismological techniques. These include wide-angle P-wave reflections **(**e.g., Kaila & Krishna, 1992), surface wave tomography (e.g., Kumar et al., 2021; Mitra et al., 2006; Mohan et al., 1997; Priestley & McKenzie, 2006; Bhattacharya, 1981) body-wave tomography (e.g., Kennett & Widiyantoro, 1999; Singh et al., 2014; Van Der Voo et al., 1999) and receiver function studies (e.g., Gaur & Priestley, 1997; Gupta et al., 2003; Julià et al., 2009; Rai et al., 2003) . There is a general consensus about the upper crustal structure among these studies but the upper mantle structure remains controversial. Estimation of velocities, thickness of the lithosphere, and extent of the lithospheric keels in the asthenosphere are some of the main reasons behind the controversy. On one hand, the Indian cratonic lithosphere is found to be anomalously thin (~100 Km) compared to the lithosphere of the other Archean cratons (~250 Km) (e.g., Kumar et al., 2013; Mitra et al., 2006) , previous studies have attributed this thinning to the anomalously hot asthenosphere caused due to plume interactions with Indian plate during it passage over volcanic hotspots (e.g. Kumar et al., 2007) , on the other side, thermobarometric and geophysical studies in Dharwar cratons have suggested the thickness in the excess of ~200 km (e.g., Griffin et al., 2009; Naganjaneyulu et al., 2012) . This creates the incertitude about the true thickness of the lithosphere and whether the discontinuity observed in the former studies is actually the Lithosphere-Asthenosphere boundary or it is some mid-lithospheric boundary (Bodin et al., 2013) .

A study of the MTZ both in terms of its thickness as well as the topography of the bounding discontinuities (d410 & d660) is an effective way to infer the strength of the chemical and thermal perturbations in the Indian lithosphere caused due to its interaction with ancient mantle plumes. The topography of MTZ can be significant in the regions with active plate tectonics such as subduction zones and rift valleys as well as beneath actively volcanic regions. However, in intraplate settings such as India, topography will be mainly affected by the average velocities in the upper mantle (<410 km).

High-velocity anomalies with respect to those in the standard earth models such as IASP91 (Kennett & Engdahl, 1991) in the upper mantle caused by the presence of thick cold lithosphere will pull up both the discontinuities while the lower velocity anomalies will depress both the discontinuities uniformly. The thickness of the MTZ is uncorrelated with the upper mantle variations (Flanagan & Shearer, 1998) but depends on the thermal and chemical state inside of the transition zone. It has been speculated that an increase in temperature of 200°C with respect to the ambient temperature can result in a reduction of the MTZ thickness by 20-30 km (G. Helffrich, 2000) . In the subduction zones, the MTZ thickness can help in determining the destination of the subducted slab. MTZ can also act as a burial ground for ancient deep subducted slabs. These relict slabs cool the surrounding material inside the MTZ and tend to increase its thickness (e.g., Dahm et al., 2017; Duan et al., 2015; Gao & Liu, 2014) .

Several attempts have been performed to map the variations in the topography and thickness of transition zone beneath different regions in India using different amounts of datasets and with different resolutions. Results for the cratonic regions of the Indian shield indicate that MTZ beneath the Indian shield is not similar to those observed beneath the other Precambrian shields (e.g., Kiselev et al., 2008; Kosarev et al., 2013; Kumar et al., 2013) . The d410 and d660 under most of the cratonic region are close to those predicted by the IASP-91 model instead of being raised as a consequence of high-velocity anomalies in the upper mantle. Some regions such as the northwestern Deccan Volcanic Province and the Southern Granulite Terrain show a delay in passage times or depression in the discontinuities. This is suggested to be caused by the influence of plume mantle interactions in the upper mantle creating a thinner than 'normal' lithosphere beneath these regions (Kumar et al., 2007) . Beneath the Himalayan foredeep, The MTZ near Delhi has been observed to be thick with raised discontinuities (Kumar et al., 2013) .

The sharpness and position of d410 and d660 can reveal significant information about the amount of water content in the transition zone. Olivine and its polymorphs can incorporate small amounts of water brought to these depths by the subducting plate. The water has the effect of stabilizing the coexistence of the two polymorphs (α & β- Olivine) across d410 over a wide range of pressure and temperatures resulting in increasing the thickness, thus decreasing the sharpness of the d410, while the opposite happens for d660 (Smyth & Frost, 2002; Wood, 1995) . The frequency dependence of the amplitude of the receiver functions corresponding to d410, sharpness of 520, and presence of low-velocity layer immediately above d410 are some of the factors that can be investigated to infer the quantity of water content (Van der Meijde et al., 2003) . To the best of our knowledge, no crucial evidence of the existence of d520 has been found beneath the Indian shield. Similarly, the presence of water inside the mantle transition zone has not been investigated in detail except in northeast India, where a study by Singh et. al. (2009) suggests the lack of wet MTZ in the region based on their observations of small frequency dependence of amplitudes of receiver functions. There have been some occasional observations of low-velocity layer atop d410 beneath a few segments of the Indian shield (Kosarev et al., 2013a; Kumar et al., 2013b; Oreshin et al., 2011) , but the extent of this feature needs to be investigated with the implications for the presence of water in the transition zone(Singh et al., 2015) .

In this study, we first utilize the P-wave receiver functions from the teleseismic waveforms recorded at 24 stations spread across the width and breadth of the country to image the topography of d410 and d660 and MTZ thickness along six linear profiles crossing a variety of geological terranes (Figure 1). We then compare the results of our study with previous studies in terms of the delay times, depths, and thickness over various regions and discuss the implications of our results for the upper mantle structure beneath the Indian shield. We then analyze the frequency dependence of amplitudes of receiver functions at d410, lookout for the presence of sharp d520 and prominent low-velocity layer atop the d410 to identify the regions beneath which relatively more volume of water can be present inside the MTZ.

2. Data and Methods

Mantle Transition Zone is most frequently studied using receiver functions (e.g. Duan et al., 2015; Gao & Liu, 2014a; Kumar et al., 2013b; Liu & Gao, 2006; Vinnik, 1977) . The receiver functions are time series obtained by deconvolving vertical component seismogram from the rotated horizontal components to isolate and amplify near receiver effects (Ammon, 1991; Langston, 1979) . When an incoming compressional P wave encounters a discontinuity during its passage through the earth from source to receiver, a fraction of it partitions into shear wave (SV) energy. On radial receiver functions, this partitioned shear wave energy appears as a relatively large amplitude positive or negative pulse depending on the nature of discontinuity and it arrives after some duration from the direct P arrival. This duration is referred to as delay time and it depends on the depth of the discontinuity and the velocity structure between the discontinuity and the receiving station. Phases corresponding to such converted shear wave energy are referred to as Pds phases with d denoting the depth of discontinuity. The P410s and P660s arrive near 45 and 70s (global average being 44.05 and 68.1s as predicted by the IASP91 model) after the direct P arrival. The exact delay times of these phases can be used to constrain the depths of discontinuities for a given velocity model.

The broadband passive seismic data used in this study was available in the form of event-based waveforms of about two hours in duration from the origin of the event and were recorded by 24 stations (Figure 1) scattered over a broad area and non-uniformly distributed over a five-year period (2007-2012). The quality and quantity of the data vary among the stations. Recording stations form a part of three networks (Figure 1), - (i) DLT - (Delhi Telemetry), (ii) RTSMN- Real-Time Seismic Monitoring Network, and (iii) Other Broadband Digital (OBD). These networks are operated by several observatories that come under the India Meteorological Department; a nodal agency of the Government of India, primarily responsible for the monitoring of seismicity and related activities throughout the country. Event-based waveforms were requested using the following criteria - (i) Epicentral distance of 30-90º, (ii) Maximum depth of 300 km, and (iii) Minimum magnitude of 5.5. The obtained seismograms were then filtered using a Butterworth four corner bandpass filter of 0.05-0.15 Hz. The frequency band was selected as the one which gave the best result after observing the results of extensive testing on different frequency bands (Figure 2 ~~5~~).

A signal-to-noise (SNR) based selection was applied to select high-quality waveforms. SNR is defined here as $\max(|A_s|)/|A_n|$, where $\max(|A_s|)$ is the maximum absolute amplitude on the vertical component in the time window of 8s prior and 12s after the predicted theoretical P-wave arrival time calculated using IASP91 velocity model and $|A_n|$ is the mean of the absolute amplitude of the waveform 10-20s before the predicted P-wave arrival time. All the waveforms having SNR>4.0 on the vertical component and the corresponding waveforms on the horizontal component were selected (Gao & Liu, 2014b, c) . The seismograms were rotated into LQT coordinate system (Vinnik, 1977) using the predicted incidence angle of P-arrival, and a water level deconvolution procedure (Ammon et al., 1990) with a water level value of 0.03 was applied to compute radial P receiver functions. Testing was also done for different water level values of 0.01 to 0.10, however, no significant change in the quality of receiver function was observed. The receiver functions were converted from time to depth domain using the 1D IASP-91 model.

Based on the data availability and geographical distribution of the stations, we divide the study area into six linear profiles, then divide each profile into rectangular bins with the dimension of a single bin being 520x110 Km. The dimensions are chosen after considering the lateral spread of piercing points for given stations and the Fresnel width of PdS in the transition zone. Figure 3 shows one such example of the division of a profile into rectangular bins. The piercing points at the depth of 535 km (middle of MTZ) were computed from ray tracing using the IASP-91 model and all the receiver functions whose piercing points lie in the same bin were moveout corrected and linearly stacked. The number of piercing points in a given bin varies from 2 to 65.

For each bin, a bootstrap resampling procedure (e.g. Gao & Liu, 2014c) with 50 iterations was applied to compute the mean and standard deviation of d410 and d660 in each bin. In each iteration, depths of d410 and d660 were picked as the depths corresponding to the maximum amplitude of receiver function within a depth window of ±30 km from 410 km and 660 km respectively. The final depths in each bin were then computed by taking an average of the results of all iterations.

3. Results & Discussion

The observed d410 depths for the entire study area range from 386 km to 421 km with a mean value of 407.7±5.9 km while d660 depths range from 630 km to 675 km with a mean value of 655.9±8.9 km. The observed MTZ thickness varies from 228.37 km to 266 km with a mean value of 248.25±8.3 km. This means MTZ depth is very close to the estimated globally averaged MTZ thickness of 250 Km. However, since time to depth conversion was done using the 1-D earth model (IASP-91), the above depths that we obtained are apparent rather than true depths. The apparent depths of d410 and d660 are a function of temperature anomalies, the existence of ~~a~~ hydrated minerals, and velocity anomalies above these discontinuities. If the true velocities are higher than the assumed velocities, the apparent depths will be pulled upward relative to true depths and vice versa. Further, apparent depths of both the discontinuities are equally affected by the velocity anomalies in the crust and upper mantle (i.e. above 410 km) while the anomalies inside the MTZ will only affect the apparent depth of d660. If the apparent depths of d410 and d660 are well correlated, it may mean that the MTZ is more uniform and the true depths vary insignificantly (Cottaar & Deuss, 2016; Gao & Liu, 2014c; Yu et al., 2021) . Alternatively, a high correlation is also observed in the case of ~~a~~ high temperature anomalies that create a positive Clapeyron slope for both the discontinuities and thus raise the apparent depths, however, this case is unlikely for the Indian shield. In our case, the correlation coefficient of the whole profile between the apparent depths of d410 and d660 comes out to be 0.43 (Figure 2). Only profile 1 and profile 4 show a high correlation between apparent depths of d410 and d660 as indicated by the correlation coefficient (CC) values. While profile 1 has a small extent suggesting the possibility of relatively homogeneous MTZ, profile 4, which extends to a length of over 2300 Kms, suggests the possibility of high compositional anomalies in the MTZ. The CC for other profiles in the study area are close to zero, suggesting the main cause of variation in apparent depths comes from velocity anomalies, water content, or thermal anomalies inside the MTZ. Table 1 shows the profile-wise apparent depths and related statistics in the study area. Given the amount of data, size of the bins used and the density of stations in our study, we do not focus on the individual bin measurements but rather analyze the average profile-wise and regional variations in the apparent depths of d410, d660 and MTZ thickness.

3.1 Correlation with Surface Geology

In general, MTZ beneath cratonic regions with deep lithospheric roots is expected to be relatively thick owing to the cold thermal nature and opposite signs of the Clapeyron slope at the two boundaries (Chevrot et al., 1999; Flanagan & Shearer, 1998; Lawrence & Shearer, 2006) . In the following paragraphs results of receiver function analysis are compared with the geology of the area through which various profiles pass.

Profile 6 (Figures 1 & 3) traverses through the Western Dharwar Craton (WDC) with Deccan Volcanic Province (DVP) in north (stations BOM, PUNE, KARD), Dharwar Schists in the middle (stations GOA, MNGR) and Southern Granulite Terrain (SGT) in the south (stations KOD, TRVM). The upper mantle structure beneath this craton is different than most other cratons of the same age. The lithosphere is relatively thin with an average thickness of ~100 km and the seismic wave velocities in the upper mantle are found to be very close to the IASP-91 earth model (e.g. Kiselev et al., 2008; Oreshin et al., 2011; Rai et al., 2003) . Unlike some other Archean cratons, where the delay times of converted phases at d410 and d660 are found to arrive as earlier as 2s compared to that obtained for the IASP-91 model, previous studies have found the delay times beneath this craton almost equal to that obtained using IASP-91 model (Chevrot et al., 1999) . The average apparent depths and MTZ thickness found for this profile in our study, i.e. 409 km, 661 km, and 252 km are very close to the global average and in ~~a~~ good agreement with previous studies, additionally confirming the anomalous nature of Transition Zone beneath Western Dharwar Craton.

A dedicated study for the mantle transition zone beneath the Southern DVP (Kumar & Mohan, 2005) using a linear array of six stations in the region between the Narmada rift and Karad with piercing points falling in nearly the same locations as ours estimated the average apparent depths for d410 and d660 to be 413 km and 665 km and MTZ thickness of 252 km, which is close to the global average. Based on these observations, they concluded that the MTZ beneath DVP is largely uniform and is unaffected by any velocity anomalies at depths less than 410 km. The body wave tomographic studies suggest the presence of a high-velocity anomaly in the upper mantle beneath most of the DVP, this high-velocity anomaly is attributed to the depletion of the upper mantle (Singh et al., 2014) . In our studies, we found the average apparent depths for d410 and d660 and MTZ thickness beneath DVP equal to 409 km, 665 km, and 256 km respectively. The values are very close to the global average with slightly thick MTZ. we suggest that the large positive anomaly observed in the upper mantle in previous studies indeed penetrates the MTZ but its strength and extent decrease with depth.

The segment of profile 6 (Figures 1 & 3) lying between Mangalore and Trivandrum falls under Southern Granulite Terrain and show~~s~~ ~~an~~ average apparent depths for d410 and d660 of 407 km and 657 km and MTZ thickness of 250 km. Previous studies have found a presence of a thinned lithosphere and low velocities in the upper mantle in this region (Gupta et al., 2003; Kosarev et al., 2013a; Kumar et al., 2014) . The low velocities are attributed to the effect of the Marion plume responsible for the separation of Madagascar from India. The MTZ in our study is found to be thinnest near Kodaikanal and Trivandrum with values being 241 and 244 Km.This is consistent with the results of a previous study by Kumar et. al. (2013).

Profile 4 (Figures 1 & 3) passes through the Eastern Ghats Mobile Belt (EGMB) in the north and middle and Southern Granulite Terrain in the south. However, the piercing points mostly fall on the side of oceanic MTZ. Our observations for this profile corroborate with the results of the previous study (Sharma & Ramesh, 2013) which focused on the Eastern Dharwar Craton and EGMB in terms of d410 and d660 showing large sporadic undulations. The MTZ thickness beneath northern EGMB appears thin with d410 being depressed and d660 being raised than their global averages. This suggests the presence of high-temperature anomalies in both the upper mantle as well as inside of the transition zone. Previous studies indicate the presence of high-temperature anomalies inside the upper mantle and attribute them to the passage of the Indian plate over a few hotspots (Kosarev et al., 2013a; Kumar et al., 2007; Negi et al., 1986) .

Profile 1 (Figures 1 & 3) lies in the northwestern part of the Himalayas with most of its piercing points lying north of the Main Boundary Thrust (MBT). The average apparent depths of d410, d660 and MTZ thickness for this profile come out to be 412 km, 659 km, and 246 km respectively. Tomographic images for this place show low-velocity anomalies in the upper mantle (Singh et al., 2014) . We suspect these anomalies extend all the way inside of the MTZ. The results for profile 2, which runs from the Himalayas to Aravali ranges through the foredeep show somewhat similar values with average apparent depths for d410 and d660 and thickness of MTZ being 412, 657, and 244 km respectively.

Profile 3 (Figures 1 & 3) between Bilaspur and Bokaro shows a thinned MTZ of 243 km with slightly raised d410 of 405 km and highly raised d660 of 649 km. This unproportionate raising of MTZ suggests the presence of high-velocity anomalies inside the MTZ beneath this region. Rest of the profile 3 passes through the same regions as profile 5 and 6 and show similar results as theirs.

Profile 5 (Figures 1 & 3) passes through Archean Aravali craton in the north (AJMR), the Northern section of DVP (BHPL), and Bastar craton (NGP) in the middle while cutting through Narmada Son Lineament and Proterozoic Eastern Ghat Mobile Belt in the south (VISK). Previous studies suggest the presence of low-velocity anomalies in the upper mantle beneath the Aravali craton (Singh et al., 2014) . Whether or not, these anomalies extend to MTZ is unclear. Our observations indicate an MTZ thickness of 254 km, with raised d410 at 406 and d660 at 660 km. A slightly lifted d410 and a normal d660 may suggest the presence of a weak low-temperature anomaly or the presence of water inside the MTZ. For the DVP and Bastar craton, apparent depths and MTZ thickness are found to be near their global averages, suggesting the high-velocity anomalies observed in the upper mantle beneath this region do not extend to the transition zone. MTZ thickness along the segment of this profile near EGMB (VISK) progressive increases as one move towards the Bay of Bengal with an average value of 248 km. Previous studies suggest the presence of a relict subducted slab at this location between the depths of 160 to 220 Km. (Sharma & Ramesh, 2013) , If such a subducted slab is present, this will result in high average upper mantle velocities, consequently resulting in the pulling up of both apparent depths. Our results do not show agreement with this as both the apparent depths are close to their average values.

3.2 Water in the Transition Zone

Water can be transported into the deep mantle in the form of hydrous minerals present in the deep subducting plate (Ohtani et al., 2004) . The water storage capacity of the upper and lower mantle is less than ~ 0.2 wt% while that of the minerals present inside the MTZ ranges from 1-3 wt% (Kohlstedt et al., 1996) . This makes the mantle transition zone a potential water reservoir. There are a number of ways in which water can affect the transition zone - (i) It can thicken the d410 while sharpening the d520 and d660, (ii) It can uplift the d410 and increase the thickness of the transition zone, and (iii) It can cause the partial melting atop the d410. We conduct tests to infer the presence of water on the basis of the nature of d520. They are frequency dependence of amplitudes of receiver functions and the presence of low-velocity layers atop the d410.

3.2.1. Frequency Dependence of Amplitudes

The presence of water can increase the thickness of the Olivine-Wadsleyite transition zone which would result in the frequency dependence of amplitudes of receiver functions at this depth. A mere 500-700 ppm by weight of the water can increase the thickness of d410 by 20-30 km (Wood,

1995) . It would also cause d520 and d660 to sharpen and can increase the overall thickness of the transition zone as well. Alternatively, the presence of low-temperature anomalies can also thicken the d410, but their effect on the thickness of the transition zone is much smaller than water. For example, a temperature reduction of 800K would only thicken the d410 by 10 km (Helffrich & Wood, 1996) , such temperature anomalies are unrealistic in the case of the Indian shield. We computed the maximum amplitudes of receiver functions in the interval of +/-50 km at d410 and d660 at different frequencies by applying a bandpass filter with a fixed lower limit of 0.05 Hz and varying upper limits of 0.75, 0.62, 0.50, 0.40, 0.35, 0.30, 0.25, 0.20 and 0.15 Hz for each individual station as done in previous studies (Van der Meijde et al., 2003) . Stations AJMR, AKL, BHPL, BLSP, BOM, BOKR, GOA, MDRS, SMLA, and VISK show high dependence of amplitudes of d410 on frequencies as displayed by negative correlation coefficients of amplitude > 0.5 (Figures 4, 5). The dependence of amplitudes of d660 for these stations is very similar but slightly less in terms of correlation coefficient except for the stations of AKL, BOKR, GOA, and MDRS where amplitudes of d660 show little dependency. Among the stations showing high-frequency dependence of amplitudes, only AKL, BOM, and SMLA show depressed d410.

3.2.2 Low-Velocity Layer Atop 410 km Discontinuity

The water solubility of the minerals inside the transition zone (~1-3%) is far greater than the water solubility of minerals in the upper and lower mantle (~0.1%). When the water from MTZ penetrates into the upper mantle, partial melting can occur as a consequence of reduced melting temperature. This partial melt of the upper mantle is dense and settles atop the d410. This has been confirmed by geophysical experiments (e.g. Huang et al., 2005) as well as geological studies (Bercovici & Karato, 2003) . We observe a consistent low-velocity layer in profile 5, from AJMR to VISK, between BOM to GOA in profile 6, and between LATR to BOM in profile 3 (Figures 1 & 3). Additionally, profile 2 shows some signs of a weak LVL near Delhi and in Bastar craton (BOKR).

Low-velocity layer atop d410 in DVP and EDC has also been reported in some previous studies such as Kosarev et. al. (2013) and Oreshin et. al. (2011). Singh et. al. (2013a) observed prominent LVL near AJMR and AKL, while a weaker LVL for some stations in DVP and EDC. Oreshin et. al. (2011) suggest the subduction-related fluids or mantle upwelling could be the reason for the presence of LVL while Singh et. al. (2013a) suggest that while the possibility of a ‘wet’ MTZ cannot be ignored, mid mantle discontinuity caused as a result of plume-upper mantle interaction is more favorable explanation for this LVL.

3.2.3 520 km Discontinuity

Knowledge of the nature and topography of mid-transition zone discontinuity or d520 is crucial to understanding the possible compositional and thermal variations inside the MTZ. Some studies advocate for its global occurrence while others claim that it is only found in certain regions and is absent beneath continental shields (Deuss & Woodhouse, 2001) . Previous studies did not find compelling evidence of a d520 beneath the Indian shield (Kosarev et al., 2013b; Kumar et al., 2013b; Oreshin et al., 2011) . In our results, we observe a persistent laterally varying mid-transition discontinuity (Figure 3). The reason behind the appearance of d520 in our study could be (i) the frequency band we use (0.05-0.15 Hz) where we do not include the long period noise or (ii) the signal-to-noise ratio we have used. The discontinuity appears either as a single reflection between depths of 530-580 km beneath the stations present in the SGT (KOD, GOA, and MDRS) and other individual stations such as VISK, BOKR, and BWNR near the east coast of India or as a double reflection between the apparent depths of 510-530 km and 560-600 km at the rest of the stations. The splitting is attributed to be caused by the compositional and thermal variations in the transition zone from the ambient conditions.

Mineral physics indicates that there are actually two transitions that may occur inside the MTZ. Apart from the usual Wadsleyite-Ringwoodite transformation, the transformation among non-Olivine components also occurs where Majorite Garnet transforms to Ca-rich Perovskite (Deuss & Woodhouse, 2001) . The Clapeyron slope of former reaction is 4.0 Mpa/K (Ringwood, 1970) while that of the latter varies from 0 to -2 Mpa/K (Ita & Stixrude, 1992; Koito et al., 2000) . In the presence of an average mantle temperature of 1500K both the transformation would occur at the same depth and a single reflection would be observed. In the presence of temperature anomalies, both the transformation would move to different depths owing to different Clapeyron slopes. Additionally, compositional variations would also contribute to the location and sharpness of both the transformations, The Wadsleyite-Ringwoodite transformation would not occur in the presence of a high Fe content while the Garnet-Perovskite would not occur in the presence of a low Ca content (Karato et al., 2000) . Other components such as water would increase the sharpness of the Wadsleyite-Ringwoodite transformation zone and favor the splitting (Inoue et al., 1998) . The lack of splitting of the waveform at d520 can therefore indicate a Ca-poor, Fe-rich or dry mantle compositional conditions. In the case of SGT, Fe-rich upper mantle and dry mantle conditions likely appears to be the case as is confirmed by previous studies. The strongest single reflection is observed at GOA and BWNR, while the single reflections beneath the other stations split into multiple reflections with increasing frequency. The stations AJMR, DDI, and SMLA show very weak mid-transition zone reflections as observed in previous studies.

Based on the evidence from the nature of d410 and d520, the frequency dependence of the amplitude of receiver functions, and the presence of low-velocity layers, we demarcate the regions possibly containing relatively more amounts of water inside the MTZ (Figure 6). Most of these regions lie in Southern Deccan Volcanic Province, Aravali craton, and Eastern Ghats Mobile Belt. Although the amount of data and the station coverage in our study limits our analysis, these regions should certainly be further investigated using dense station coverage and a more realistic velocity model.

4. Conclusion

Our analysis reveals the heterogeneous nature of the mantle transition zone beneath the Indian shield. The MTZ thickness beneath most of the cratons is close to global averages and in good agreement with the results of previous studies. The high-velocity anomalies extend to the mantle transition zone beneath some regions in southern Deccan Volcanic Province. A persistent and laterally varying mid transition zone discontinuity is observed beneath all the profiles. Most stations show significant dependence of amplitudes of receiver functions on frequency. Low velocity layer just above the 410 km discontinuity is observed in profile 5 and beneath some regions in Deccan Volcanic Province and Eastern Ghats Mobile Belts. Based on these evidences, we mark some regions that show the possibility of 'wet' MTZ and should further be investigated using dense station coverage and a more realistic velocity model.

5. Acknowledgements

We are thankful to India Meteorological Department (IMD) for providing us with the required waveform data. Receiver functions were computed using a python based 'rf' package (Eulenfeld, 2020) . All the additional processing was done using Obspy (Krischer et al., 2015) . All the maps were plotted using PyGMT(Uieda et al., 2021) . No funding was obtained for carrying out this work from any funding agency.

6. References

Ammon, C. J. (1991). The isolation of receiver effects from teleseismic P waveforms. *Bulletin - Seismological Society of America*, *81*(6), 2504–2510. https://doi.org/10.1785/BSSA0810062504

Ammon, C. J., Randall, G. E., & Zandt, G. (1990). On the nonuniqueness of receiver function inversions. *Journal of Geophysical Research*, *95*(B10). https://doi.org/10.1029/JB095IB10P15303

Bercovici, D., & Karato, S. I. (2003). Whole-mantle convection and the transition-zone water filter. *Nature*, *425*(6953), 39–44. https://doi.org/10.1038/NATURE01918

Bina, C., Solid, G. H.-J. of G. R., & 1994, undefined ??. (1994). Phase transition Clapeyron slopes and transition zone seismic discontinuity topography. *Wiley Online Library*, *99*(B8), 853–868. https://doi.org/10.1029/94JB00462

Bodin, T., Yuan, H., & Romanowicz, B. (2013). Inversion of receiver functions without deconvolution-application to the Indian craton. *Geophysical Journal International*, *196*(2), 1025–1033. https://doi.org/10.1093/GJI/GGT431

Chevrot, S., Vinnik, L., & Montagner, J. P. (1999). Global-scale analysis of the mantle Pds phases. *Journal of Geophysical Research: Solid Earth*, *104*(B9), 20203–20219. https://doi.org/10.1029/1999JB900087

Cottaar, S., & Deuss, A. (2016). Large-scale mantle discontinuity topography beneath Europe: Signature of akimotoite in subducting slabs. *Journal of Geophysical Research: Solid Earth*, *121*(1), 279–292. https://doi.org/10.1002/2015JB012452

Dahm, H. H., Gao, S. S., Kong, F., & Liu, K. H. (2017). Topography of the Mantle Transition Zone Discontinuities Beneath Alaska and Its Geodynamic Implications: Constraints from Receiver Function Stacking. *Journal of Geophysical Research: Solid Earth*, *122*(12), 10,352-10,363. https://doi.org/10.1002/2017JB014604

Deuss, A., & Woodhouse, J. (2001). Seismic observations of splitting of the mid-transition zone discontinuity in Earth's mantle. *Science*, *294*(5541), 354–357. https://doi.org/10.1126/SCIENCE.1063524/SUPPL_FILE/1063524S2_THUMB.GIF

Drury, S. A., Harris, N. B. W., Holt, R. W., Reeves-Smith, G. J., & Wightman, R. T. (1984). Precambrian tectonics and crustal evolution in south India. *Journal of Geology*, *92*(1), 3–20. https://doi.org/10.1086/628831

Duan, Y., Tian, X., Liu, Z., Zhu, G., & Nie, S. (2015). Lithospheric detachment of India and Tibet inferred from thickening of the mantle transition zone. *Journal of Geodynamics*, *97*, 1–6. https://doi.org/10.1016/j.jog.2016.02.001

Eulenfeld, T. (2020). rf: Receiver function calculation in seismology. *Journal of Open Source Software*, *5*(48), 1808. https://doi.org/10.21105/JOSS.01808

Flanagan, M. P., & Shearer, P. M. (1998). Global mapping of topography on transition zone velocity discontinuities by stacking SS precursors. *Journal of Geophysical Research: Solid Earth*, *103*(B2), 2673–2692. https://doi.org/10.1029/97JB03212

Gaina, C., Müller, R. D., Brown, B., Ishihara, T., & Ivanov, S. (2007). Breakup and early seafloor spreading between India and Antarctica. *Geophysical Journal International*, *170*(1), 151–169. https://doi.org/10.1111/J.1365-246X.2007.03450.X

Gao, S. S., & Liu, K. H. (2014a). Imaging mantle discontinuities using multiply-reflected P-to-S conversions. *Earth and Planetary Science Letters*, *402*(C), 99–106. https://doi.org/10.1016/J.EPSL.2013.08.025

Gao, S. S., & Liu, K. H. (2014b). Imaging mantle discontinuities using multiply-reflected P-to-S conversions. *Earth and Planetary Science Letters*, *402*(C), 99–106. https://doi.org/10.1016/j.epsl.2013.08.025

Gao, S. S., & Liu, K. H. (2014c). Mantle transition zone discontinuities beneath the contiguous United States. *Journal of Geophysical Research: Solid Earth*, *119*(8), 6452–6468. https://doi.org/10.1002/2014JB011253

Gaur, V. K., & Priestley, K. F. (1997). Shear wave velocity structure beneath the Archaean granites around Hyderabad, inferred from receiver function analysis. *Proceedings - Indian Academy of Sciences, Earth and Planetary Sciences*, *106*(1–2), 1–8. https://doi.org/10.1007/BF02841745

Ghosh, S., Ohtani, E., Litasov, K. D., Suzuki, A., Dobson, D., & Funakoshi, K. (2013). Effect of water in depleted mantle on post-spinel transition and implication for 660km seismic discontinuity. *Earth and Planetary Science Letters*, *371–372*, 103–111. https://doi.org/10.1016/J.EPSL.2013.04.011

Griffin, W. L., Kobussen, A. F., Babu, E. V. S. S. K., O'Reilly, S. Y., Norris, R., & Sengupta, P. (2009). A translithospheric suture in the vanished 1-Ga lithospheric root of South India: Evidence from contrasting lithosphere sections in the Dharwar Craton. *Lithos*, *112*, 1109–1119. https://doi.org/10.1016/J.LITHOS.2009.05.015

Gupta, S., Rai, S. S., Prakasam, K. S., Srinagesh, D., Bansal, B. K., Chadha, R. K., Priestley, K., & Gaur, V. K. (2003). The nature of the crust in southern India: Implications for Precambrian crustal evolution. *Geophysical Research Letters*, *30*(8). https://doi.org/10.1029/2002GL016770

Helffrich, G. (2000). Topography of the transition zone seismic discontinuities. *Reviews of Geophysics*, *38*(1), 141–158. https://doi.org/10.1029/1999RG000060

Helffrich, G. R., & Wood, B. J. (1996). 410 km discontinuity sharpness and the form of the olivine α-β phase diagram: resolution of apparent seismic contradictions. *Geophysical Journal International*, *126*(2), F7–F12. https://doi.org/10.1111/J.1365-246X.1996.TB05292.X

Huang, X., Xu, Y., & Karato, S. I. (2005). Water content in the transition zone from electrical conductivity of wadsleyite and ringwoodite. *Nature*, *434*(7034), 746–749. https://doi.org/10.1038/NATURE03426

Inoue, T., Weidner, D. J., Northrup, P. A., & Parise, J. B. (1998). Elastic properties of hydrous ringwoodite (γ-phase) in Mg2SiO4. *Earth and Planetary Science Letters*, *160*(1–2), 107–113. https://doi.org/10.1016/S0012-821X(98)00077-6

Ita, J., & Stixrude, L. (1992). Petrology, elasticity, and composition of the mantle transition zone. *Journal of Geophysical Research*, *97*(B5), 6849–6866. https://doi.org/10.1029/92JB00068

Jay, A. E., & Widdowson, M. (2008). Stratigraphy, structure and volcanology of the SE Deccan continental flood basalt province: Implications for eruptive extent and volumes. *Journal of the Geological Society*, *165*(1), 177–188. https://doi.org/10.1144/0016-76492006-062

Julià, J., Jagadeesh, S., Rai, S. S., & Owens, T. J. (2009). Deep crustal structure of the Indian shield from joint inversion of P wave receiver functions and Rayleigh wave group velocities: Implications for Precambrian crustal evolution. *Journal of Geophysical Research: Solid Earth*, *114*(10). https://doi.org/10.1029/2008JB006261

Karato, S., Forte, A., Liebermann, R., Masters, G., & Stixrude, L. (2000). Earth's Deep Interior: Mineral Physics and Tomography From the Atomic to the Global Scale. *GMS*, *117*. https://doi.org/10.1029/GM117

Kennett, B. L. N., & Engdahl, E. R. (1991). Traveltimes for global earthquake location and phase identification. *Geophysical Journal International*, *105*(2), 429–465. https://doi.org/10.1111/J.1365-246X.1991.TB06724.X

Kennett, B. L. N., & Widiyantoro, S. (1999). A low seismic wavespeed anomaly beneath northwestern India: A seismic signature of the Deccan plume? *Earth and Planetary Science Letters*, *165*(1), 145–155. https://doi.org/10.1016/S0012-821X(98)00260-X

Kiselev, S., Vinnik, L., Oreshin, S., Gupta, S., Rai, S. S., Singh, A., Kumar, M. R., & Mohan, G. (2008). Lithosphere of the Dharwar craton by joint inversion of P and S receiver functions. *Geophysical Journal International*, *173*(3), 1106–1118. https://doi.org/10.1111/J.1365-246X.2008.03777.X

Kohlstedt, D. L., Keppler, H., & Rubie, D. C. (1996). Solubility of water in the α, β and γ phases of (Mg,Fe)2SiO4. *Contributions to Mineralogy and Petrology*, *123*(4), 345–357. https://doi.org/10.1007/S004100050161

Koito, S., Akaogi, M., Kubota, O., & Suzuki, T. (2000). Calorimetric measurements of perovskites in the system CaTiO3-CaSiO3 and experimental and calculated phase equilibria for high-pressure dissociation of diopside. *Physics of the Earth and Planetary Interiors*, *120*(1), 1–10. https://doi.org/10.1016/S0031-9201(99)00171-5

Kosarev, G. L., Oreshin, S. I., Vinnik, L. P., Kiselev, S. G., Dattatrayam, R. S., Suresh, G., & Baidya, P. R. (2013a). Heterogeneous lithosphere and the underlying mantle of the Indian subcontinent. *Tectonophysics*, *592*, 175–186. https://doi.org/10.1016/J.TECTO.2013.02.023

Kosarev, G. L., Oreshin, S. I., Vinnik, L. P., Kiselev, S. G., Dattatrayam, R. S., Suresh, G., & Baidya, P. R. (2013b). Heterogeneous lithosphere and the underlying mantle of the Indian subcontinent. *Tectonophysics*, *592*, 175–186. https://doi.org/10.1016/J.TECTO.2013.02.023

Krischer, L., Megies, T., Barsch, R., Beyreuther, M., Lecocq, T., Caudron, C., & Wassermann, J. (2015). ObsPy: A bridge for seismology into the scientific Python ecosystem. *Computational Science and Discovery*, *8*(1). https://doi.org/10.1088/1749-4699/8/1/014003

Kumar, A., Kumar, N., Mukhopadhyay, S., Klemperer, S. L., 2021. Tomographic Image of Shear Wave Structure of NE India Based on Analysis of Rayleigh Wave Data. Front. Earth Sci. - Solid Earth Geophysics (special volume on Mountain Building). 9:680361, https://doi.org/10.3389/feart.2021.680361.

Kumar, M. R., Saikia, D., Singh, A., Srinagesh, D., Baidya, P. R., & Dattatrayam, R. S. (2013a). Low shear velocities in the sub-lithospheric mantle beneath the Indian shield? *Journal of Geophysical Research: Solid Earth*, *118*(3), 1142–1155. https://doi.org/10.1002/JGRB.50114

Kumar, M. R., Saikia, D., Singh, A., Srinagesh, D., Baidya, P. R., & Dattatrayam, R. S. (2013b). Low shear velocities in the sub-lithospheric mantle beneath the Indian shield? *Journal of Geophysical Research: Solid Earth*, *118*(3), 1142–1155. https://doi.org/10.1002/JGRB.50114

Kumar, P., Ravi Kumar, M., Srijayanthi, G., Arora, K., Srinagesh, D., Chadha, R. K., & Sen, M. K. (2013). Imaging the lithosphere-asthenosphere boundary of the Indian plate using converted wave techniques. *Journal of Geophysical Research: Solid Earth*, *118*(10), 5307–5319. https://doi.org/10.1002/JGRB.50366

Kumar, Prakash, Yuan, X., Kumar, M. R., Kind, R., Li, X., & Chadha, R. K. (2007). The rapid drift of the Indian tectonic plate. *Nature*, *449*(7164), 894–897. https://doi.org/10.1038/NATURE06214

Kumar, R. (1985). *Fundamentals of historical geology and stratigraphy of India*. https://agris.fao.org/agris-search/search.do?recordID=US201300618802

Lawrence, J. F., & Shearer, P. M. (2006). A global study of transition zone thickness using receiver functions. *Journal of Geophysical Research: Solid Earth*, *111*(6). https://doi.org/10.1029/2005JB003973

Lebedev, S., Chevrot, S., & Van der Hilst, R. D. (2002). Seismic evidence for olivine phase changes at the 410- and 660-kilometer discontinuities. *Science*, *296*(5571), 1300–1302. https://doi.org/10.1126/SCIENCE.1069407

??lithosphere, W. M.-T. oceanic, & 1981, undefined. (n.d.). 13. Hotspot tracks and the opening of the Atlantic and Indian Oceans. *Books.Google.Com*. Retrieved March 13, 2022, from https://books.google.com/books?hl=en&lr=&id=gRZihrnakJoC&oi=fnd&pg=PA443&ots=W8r6e8aT3R&sig=YGLMBR6uPQ-Nx8zCCkzz1-YY7Ds

Liu, K. H., & Gao, S. S. (2006). Mantle transition zone discontinuities beneath the Baikal rift and adjacent areas. *Journal of Geophysical Research: Solid Earth*, *111*(11). https://doi.org/10.1029/2005JB004099

McKenzie, D., & Sclater, J. G. (1971). The Evolution of the Indian Ocean since the Late Cretaceous. *Geophysical Journal of the Royal Astronomical Society*, *24*(5), 437–528. https://doi.org/10.1111/J.1365-246X.1971.TB02190.X

Meert, J. G., Pandit, M. K., Pradhan, V. R., Banks, J., Sirianni, R., Stroud, M., Newstead, B., & Gifford, J. (2010). Precambrian crustal evolution of Peninsular India: A 3.0 billion year odyssey. *Journal of Asian Earth Sciences*, *39*(6), 483–515. https://doi.org/10.1016/J.JSEAES.2010.04.026

Mitra, S., Priestley, K., Gaur, V. K., & Rai, S. S. (2006). Shear-wave structure of the South Indian lithosphere from Rayleigh wave phase-velocity measurements. *Bulletin of the Seismological Society of America*, *96*(4 A), 1551–1559. https://doi.org/10.1785/0120050116

Mohan, G., Rai, S. S., & Panza, G. F. (1997). Shear velocity structure of the laterally heterogeneous crust and uppermost mantle beneath the Indian region. *Tectonophysics*, *277*(4), 259–270. https://doi.org/10.1016/S0040-1951(97)00029-2

Molnar, P. (1990). S-wave residuals from earthquakes in the Tibetan region and lateral variations in the upper mantle. *Earth and Planetary Science Letters*, *101*(1), 68–77. https://doi.org/10.1016/0012-821X(90)90125-H

Naganjaneyulu, K., Sciences, M. S.-J. of A. E., & 2012, undefined. (n.d.). The nature and thickness of lithosphere beneath the Archean Dharwar Craton, southern India: a magnetotelluric model. *Elsevier*. Retrieved March 13, 2022, from https://www.sciencedirect.com/science/article/pii/S136791201100277X

Negi, J. G., Pandey, O. P., & Agrawal, P. K. (1986). Super-mobility of hot indian lithosphere. *Tectonophysics*, *131*(1–2), 147–156. https://doi.org/10.1016/0040-1951(86)90272-6

Ohtani, E., Litasov, K., Hosoya, T., Kubo, T., & Kondo, T. (2004). Water transport into the deep mantle and formation of a hydrous transition zone. *Physics of the Earth and Planetary Interiors*, *143*(1–2), 255–269. https://doi.org/10.1016/j.pepi.2003.09.015

Oreshin, S. I., Vinnik, L. P., Kiselev, S. G., Rai, S. S., Prakasam, K. S., & Treussov, A. V. (2011). Deep seismic structure of the Indian shield, western Himalaya, Ladakh and Tibet. *Earth and Planetary Science Letters*, *307*(3–4), 415–429. https://doi.org/10.1016/J.EPSL.2011.05.016

Priestley, K., & McKenzie, D. (2006). The thermal structure of the lithosphere from shear wave velocities. *Earth and Planetary Science Letters*, *244*(1–2), 285–301. https://doi.org/10.1016/J.EPSL.2006.01.008

Rai, S. S., Priestley, K., Suryaprakasam, K., Srinagesh, D., Gaur, V. K., & Du, Z. (2003). Crustal shear velocity structure of the south Indian shield. *Journal of Geophysical Research: Solid Earth*, *108*(B2). https://doi.org/10.1029/2002JB001776

Ratheesh-Kumar, R. T., Windley, B. F., & Sajeev, K. (2014). Tectonic inheritance of the Indian Shield: New insights from its elastic thickness structure. *Tectonophysics*, *615–616*, 40–52. https://doi.org/10.1016/j.tecto.2013.12.010

Ravi Kumar, M., & Mohan, G. (2005). Mantle discontinuities beneath the Deccan volcanic province. *Earth and Planetary Science Letters*, *237*(1–2), 252–263. https://doi.org/10.1016/J.EPSL.2005.06.034

Replumaz, A., Kárason, H., van der Hilst, R. D., Besse, J., & Tapponnier, P. (2004). 4-D evolution of SE Asia's mantle from geological reconstructions and seismic tomography. *Earth and Planetary Science Letters*, *221*(1–4), 103–115. https://doi.org/10.1016/S0012-821X(04)00070-6

Res., C. L.-J. geophys., & 1979, undefined. (n.d.) ??. Structure under Mount Rainer, Washington, inferred from teleseismic body waves. *Ci.Nii.Ac.Jp*. Retrieved March 13, 2022, from https://ci.nii.ac.jp/naid/10030810990/

Ringwood, A. E. (1968). Phase transformations in the mantle. *Earth and Planetary Science Letters*, *5*(C), 401–412. https://doi.org/10.1016/s0012-821x(68)80072-x

Ringwood, A. E. (1970). Phase transformations and the constitution of the mantle. *Physics of the Earth and Planetary Interiors*, *3*(C), 109–155. https://doi.org/10.1016/0031-9201(70)90047-6

Sharma, S. Das, & Ramesh, D. S. (2013). Imaging mantle lithosphere for diamond prospecting in southeast India. *Lithosphere*, *5*(4), 331–342. https://doi.org/10.1130/L269.1

Singh, A., Mercier, J. P., Ravi Kumar, M., Srinagesh, D., & Chadha, R. K. (2014). Continental scale body wave tomography of India: Evidence for attrition and preservation of lithospheric roots. *Geochemistry, Geophysics, Geosystems*, *15*(3), 658–675. https://doi.org/10.1002/2013GC005056

Singh, A., Singh, C., & Kennett, B. L. N. (2015). A review of crust and upper mantle structure beneath the Indian subcontinent. *Tectonophysics*, *644*, 1–21. https://doi.org/10.1016/j.tecto.2015.01.007

Smyth, J. R., & Frost, D. J. (2002). The effect of water on the 410-km discontinuity: An experimental study. *Geophysical Research Letters*, *29*(10), 123-1-123–124. https://doi.org/10.1029/2001GL014418

Society, S. B.-B. of the S., & 1981, undefined. (n.d.). Observation and inversion of surface wave group velocities across central India. *Pubs.Geoscienceworld.Org*, *7*(5), 1489–1501. Retrieved March 13, 2022, from https://pubs.geoscienceworld.org/ssa/bssa/article-abstract/71/5/1489/118228

Uieda, L., Tian, D., Leong, W. J., Jones, M., Schlitzer, W., Toney, L., Grund, M., Yao, J., Magen, Y., Materna, K., Newton, T., Anant, A., Ziebarth, M., Wessel, P., & Quinn, J. (2021). *PyGMT: A Python interface for the Generic Mapping Tools*. https://doi.org/10.5281/ZENODO.5607255

Van der Meijde, M., Marone, F., Giardini, D., & Van der Lee, S. (2003). Seismic evidence for water deep in Earth's upper mantle. *Science*, *300*(5625), 1556–1558. https://doi.org/10.1126/SCIENCE.1083636

Van Der Voo, R., Spakman, W., & Bijwaard, H. (1999). Tethyan subducted slabs under India. *Earth and Planetary Science Letters*, *171*(1), 7–20. https://doi.org/10.1016/S0012-821X(99)00131-4

Vinnik, L. P. (1977). Detection of waves converted from P to SV in the mantle. *Physics of the Earth and Planetary Interiors*, *15*(1), 39–45. https://doi.org/10.1016/0031-9201(77)90008-5

Wood, B. J. (1995). The effect of H2O on the 410-kilometer seismic discontinuity. *Science*, *268*(5207), 74–76. https://doi.org/10.1126/SCIENCE.268.5207.74

Yu, Y., Xu, Z., Gao, S. S., Liu, K. H., & Gao, J. (2021). Layered mantle heterogeneities associated with post-subducted slab segments. *Earth and Planetary Science Letters*, *571*. https://doi.org/10.1016/J.EPSL.2021.117115

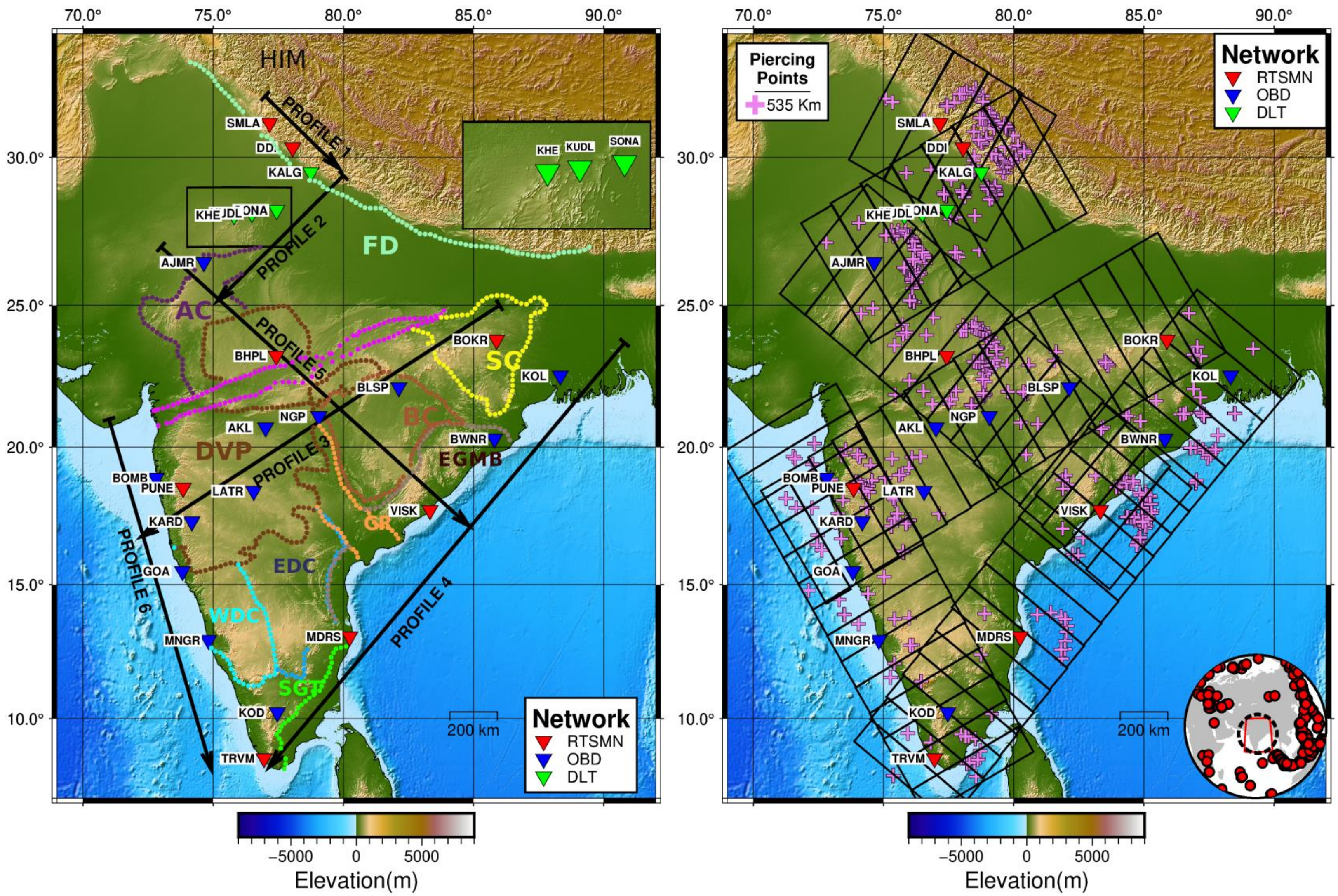

Figure 1: (a) Map showing locations of stations and the profiles used in this study. Individual geological terranes are marked by distinct colors. AC - Aravali Craton, BC – Bastar Craton, DVP – Deccan Volcanic Province, EDC – Eastern Dharwar Craton, EGMB – Eastern Ghats Mobile Belt, FD – Foredeep, GR – Godavari Rift, HIM – Himalayan range, NSL – Narmada Son Lineament, SC – Singhbhum

Craton, SGT – Southern Granulite Terrain, WDC – Western Dharwar Craton. (b) Piercing points of all the receiver functions used in this study are shown by pink crosses. Each of the profiles was divided into rectangular bins of 5°x1° in dimensions.

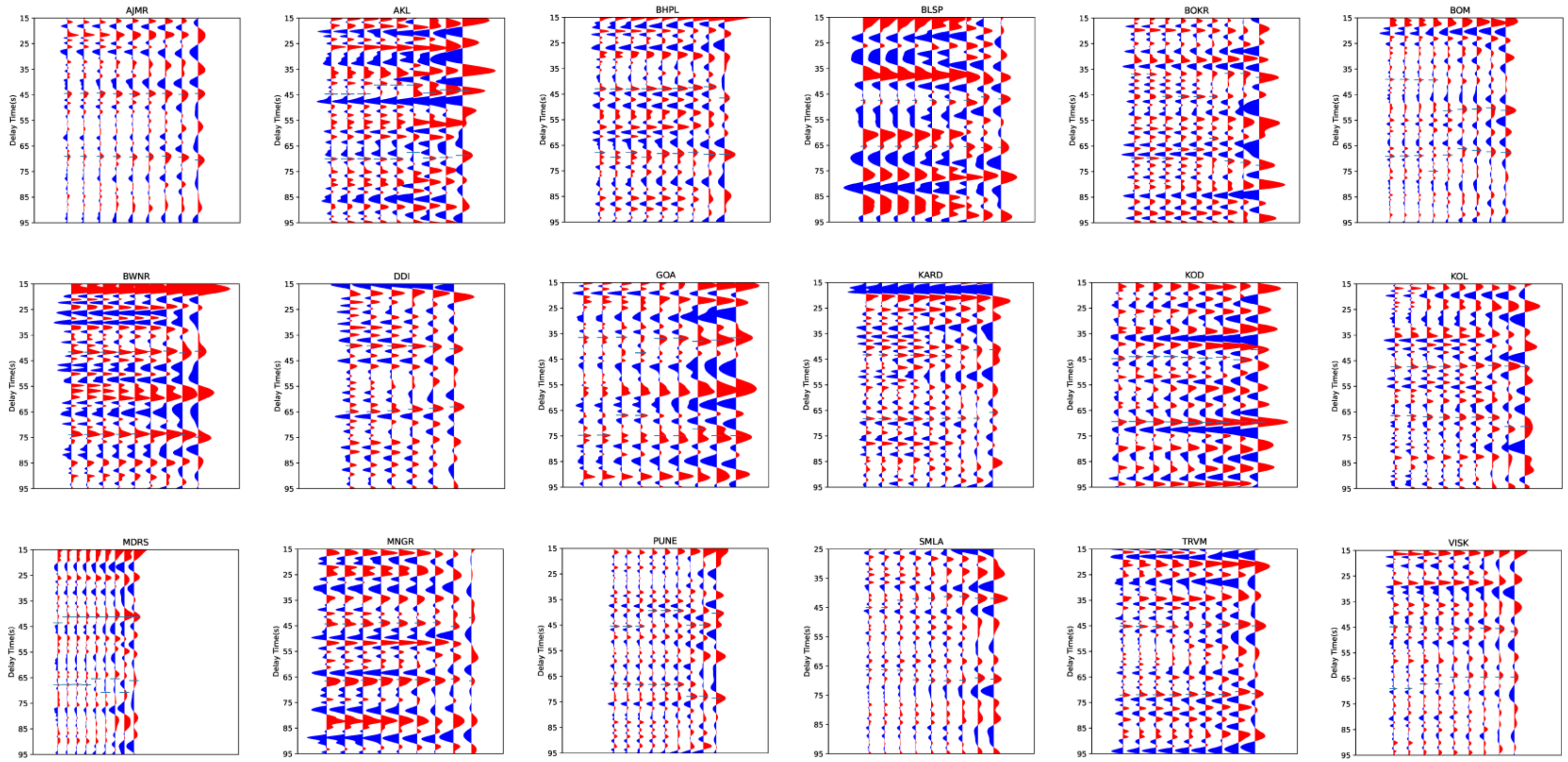

Figure 2: Frequency dependence of amplitudes of receiver functions for all the stations having a good enough signal-to-noise ratios. The amplitudes at each frequency (marked by black lines) were picked as the maximum amplitude within ±50 Km of each discontinuity.

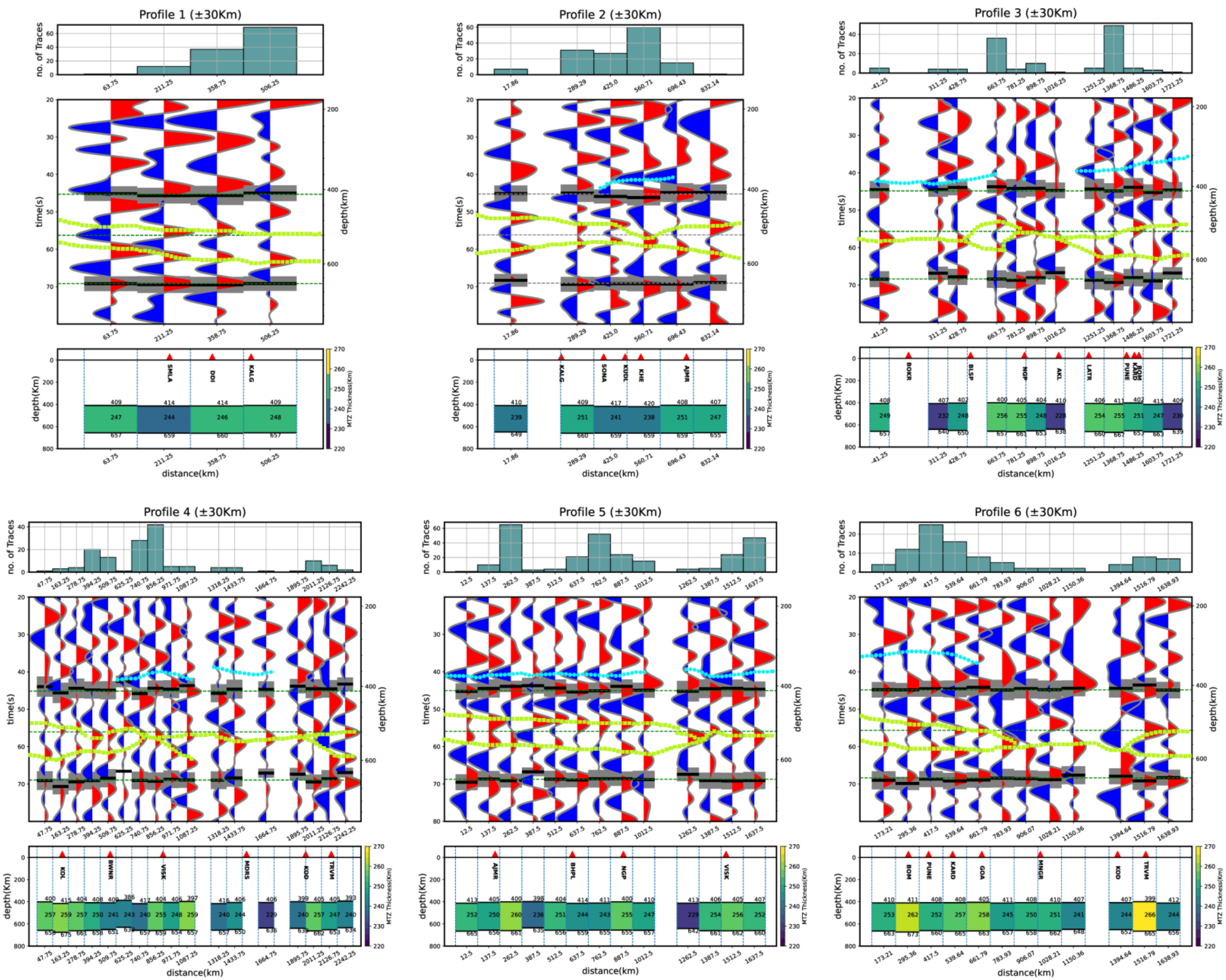

Profile 1 (±30Km)
Profile 2 (±30Km)
Profile 3 (±30Km)
Profile 4 (±30Km)
Profile 5 (±30Km)
Profile 6 (±30Km)
no. of Traces
time(s)
depth(km)
depth(Km)
distance(km)
MTZ Thickness(Km)
SHLA
DDI
KALG
SONA
KHE
AJMR
BOKR
BLSP
NGP
AKL
LATR
PUNE
KOL
BWNR
VISK
MDRS
KOD
TRVM
BHPL
BOM
KARD
GOA
MNGR

Figure 3: Results of our analysis. In each individual subplot, the top axes show the number of piercing points in each bin; the middle axes show the stacked receiver functions for each bin, the grey area near each discontinuity represents one standard deviation computed from the results of bootstrap sampling, the light blue colored dotted line atop d410 represents Low Velocity Layer, The light green colored dotted squares show mid-transition zone discontinuities; bottom axes show the topography of the d410 and d660 in each bin, color-coded by the MTZ thickness along with the stations on top.

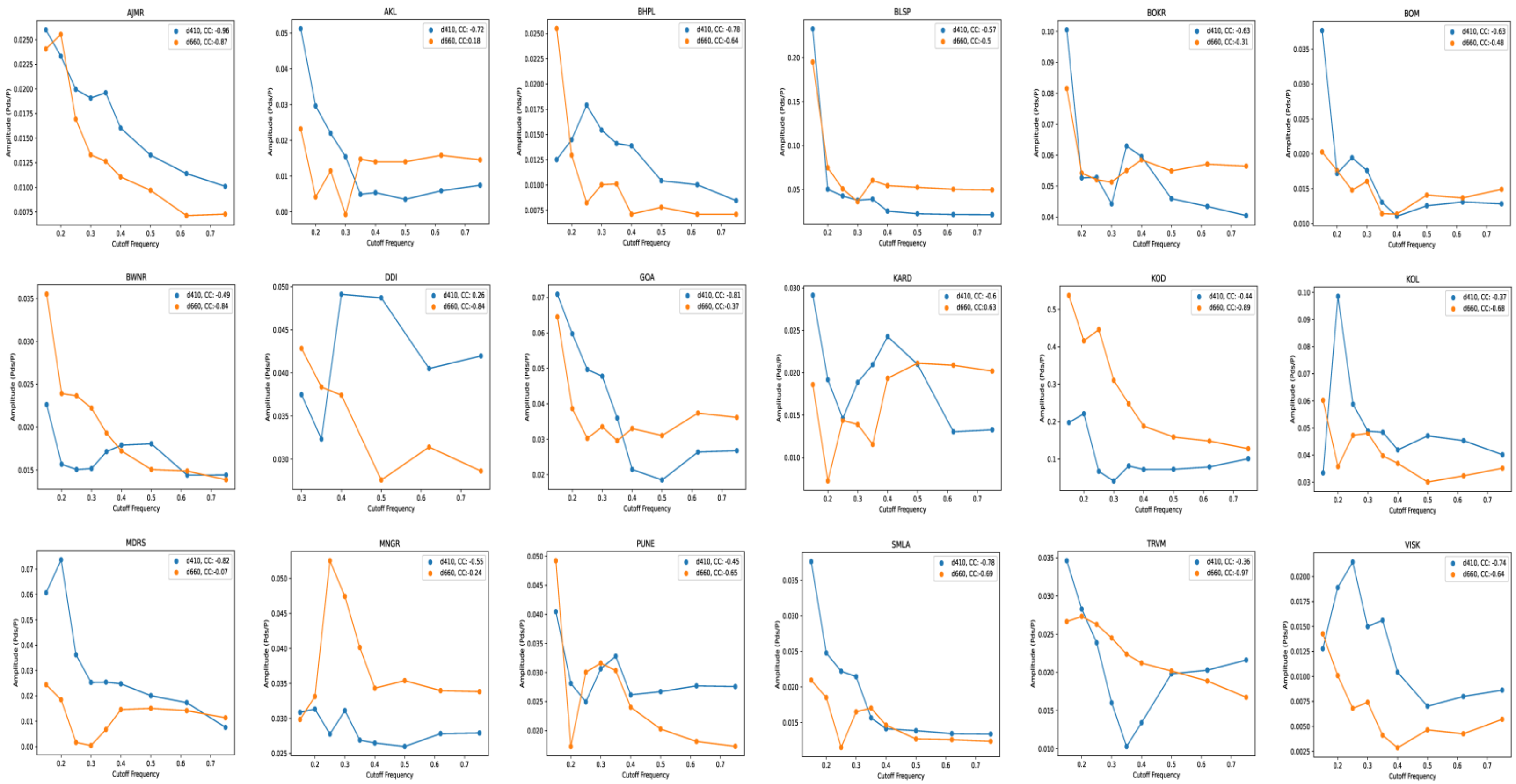

Figure 4: Frequency dependence of the amplitudes of receiver functions at d410 and d660 for all the stations used in the study except NGP, LATR, KHE, KUDL & SON, the latter stations did not show a good enough signal-to-noise ratio for reliable computation of frequency-amplitude dependence.

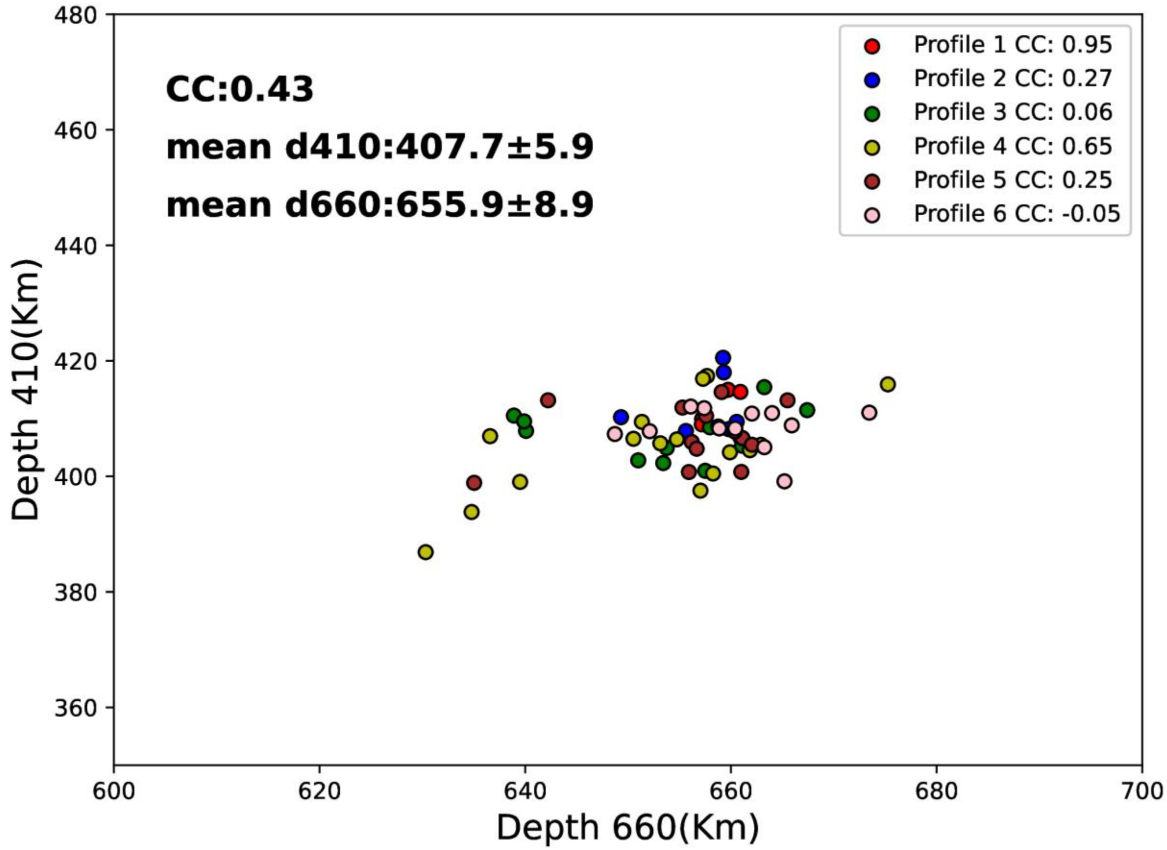

Figure 5: Relation between apparent depths of d410 and d660 for the individual profiles.

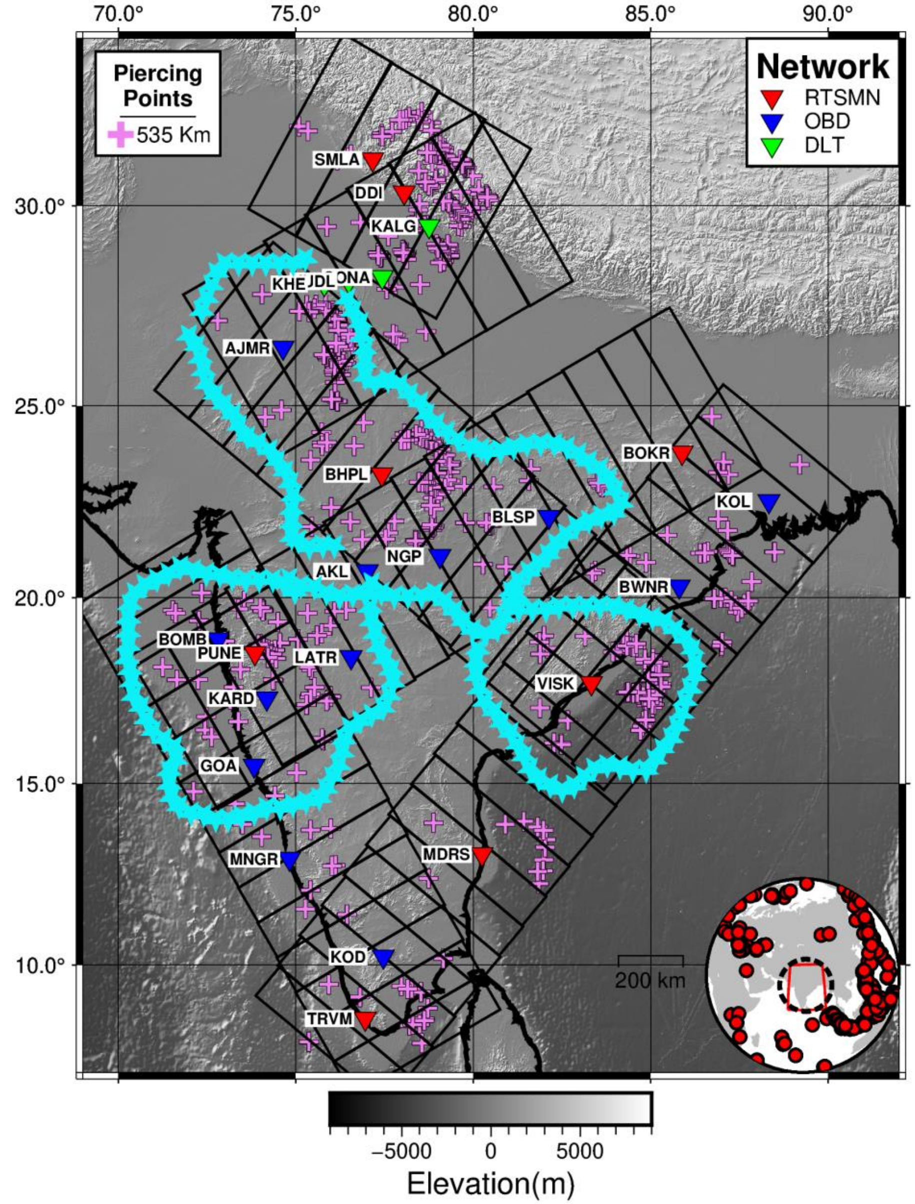

Figure 6: Regions having the strong possibility of a "wet" transition zone based on the evidence from low-velocity layer, mid-transition zone discontinuities, the frequency dependence of amplitudes of receiver functions, and nature of d41

Table 1: Values of the mean depth of d410 and d660, thickness of MTZ, number of bins, and number of RFs along with each profile.

Profile	$d410 \pm \sigma_{d410}$ (Km)	$d660 \pm \sigma_{d660}$ (Km)	$MTZ \pm \sigma_{MTZ}$ (Km)	Length (Km)	Number of bins	Number of RFs
Profile 1	412±2.68	658±1.62	247±1.27	590	4	153
Profile 2	412±5	657±3.9	245±5.43	950	6	148
Profile 3	407±4.04	654±9.2	247±9.86	1880	14	106
Profile 4	405±7.75	653±11.23	248±8.51	2310	18	168
Profile 5	407±5	656±8	249±8.33	1750	13	255
Profile 6	408.2±3.45	660±6.34	252±7.36	1710	13	92

Declaration of interests

☒The authors declare that they have no known competing financial interests or personal relationships that could have appeared to influence the work reported in this paper.

☐The authors declare the following financial interests/personal relationships which may be considered as potential competing interests: